JET-P(94)72

Topological Transitions of Fast Ion Orbits in Magnetically Confined Plasmas

F Porcelli[1], L-G Eriksson, I Furno[1].

JET Joint Undertaking, Abingdon, Oxfordshire, OX14 3EA, UK.
[1] Permanent address: Dipartimento di Energetica, Politecnico di Torino, Italy.

Preprint of a paper to be submitted for publication in
Nuclear Fusion Letters

January 1995

Abstract

Fast ion orbits decelerating in a magnetically confined plasma undergo topological transitions associated with the branching of the characteristic curves of the relevant Fokker-Planck equation. Transition probability functions are introduced. A significant inward drift as the fast ions slow down in energy is pointed out.

The question of stability and confinement of supra thermal ions with energies in the MeV range is of paramount importance to the dynamics of magnetically confined plasmas. In order to assess these issues a detailed knowledge of the fast ion distribution function is important. We are concerned with the breakdown of the standard treatment of fast ion orbits in axisymmetric toroidal confinement configurations[1], which assumes that the radial excursion of an orbit guiding centre across a magnetic surface is small compared with the distance, *r,* of this surface from the magnetic axis. The evolution of fast ion orbits with finite radial width, as these ions decelerate while colliding with the thermal electrons, has been considered by several authors[2-5]. The relevant Fokker-Planck equation is a first order partial differential equation, which is solved by the method of characteristics. We find a branching of the characteristic curves, corresponding to topological orbit transitions. This leads us to the introduction of transition probability functions, which determine the orbit evolution across the transition region.. The less frequent collisions with the thermal ions, which give rise to pitch-angle scattering in velocity space, can also induce topological orbit transitions. However, these collisions represent a diffusion process in phase space, and as such their net bias to the transition probabilities is small and will be neglected in this paper. Finally, we draw the attention to a significant radial inward drift that non-standard orbits experience as they slow down in energy.

The standard treatment of trapped particle orbits in a tokamak breaks down in the central plasma region of radius $\delta_p \equiv \Delta^{2/3} R$, where $\Delta \equiv 2q\rho / R$, ρ is the average ion Larmor radius, R is the major toroidal radius, $q(r) \approx rB_\varphi / RB_\vartheta$ is the winding index of the magnetic field lines, B_φ and B_ϑ are the toroidal and poloidal magnetic field components, respectively. Within this region, the standard *banana* orbit width [1],. $\delta_b \equiv \varepsilon^{-1/2} q\rho$, with $\varepsilon = r / R$, exceeds r. For example, for a $1MeV$ hydrogen ion and typical parameters of the JET Tokamak, $\delta_p \sim 0.3m$ is about one third of the plasma minor radius. The orbits with the largest radial widths, comparable with δ_p, are those with a parallel-to-perpendicular (with respect to the magnetic field) velocity ratio $v_\parallel / v_\perp \leq (\delta_p / R)^{1/2}$. We refer to these orbits as non-standard, or *potato* orbits[6-8]. Most of the fast ions produced by on-axis Ion Cyclotron Radio Frequency heating on JET have non-standard orbits, as the width of the ICRF deposition profile is comparable with δ_p.

In the absence of collisions, the orbit equation for the particle guiding centres can be obtained from the invariance of the particle kinetic energy, $E = mv^2/2$, magnetic moment, $\mu = mv_\perp^2/2B$, and toroidal canonical momentum, $P_\varphi = (Ze/c)\psi - mRv_\parallel B_\varphi/B$, where $\psi \geq 0$ is the poloidal magnetic flux. We consider a standard low-β Tokamak equilibrium where the flux surface cross sections depart from concentric circles by terms of order ε. To leading order in ε, let us set $v_\parallel = \sigma_\parallel v_{\perp 0}(\lambda + \varepsilon\cos\vartheta)^{1/2}$, where $\sigma_\parallel = \mathrm{sign}(v_\parallel)$, $v_{\perp 0} \equiv (2\mu B_0/m)^{1/2}$, B_0 is the value of B on axis and $\lambda \equiv (E/\mu B_0) - 1$. We introduce the dimensionless variables $\hat{r} \equiv r/\delta_p$, $\hat{\lambda} \equiv (R/\delta_p)\lambda$, $\hat{\psi} \equiv (2q_0/B\delta_p^2)\psi$ and $\hat{\psi}_\varphi \equiv (2q_0/B\delta_p^2)(cP_\varphi/Ze)$, where the characteristic potato width, $\delta_p \equiv (2q_0 v_{\perp 0}/\Omega_0 R_0)^{2/3} R_0$, is defined here as an invariant of the motion, R_0 is the distance of the magnetic axis from the torus symmetry axis, $\Omega_0 \equiv ZeB_0/mc$ and $q_0 \equiv q(0)$. We assume that the fast ions are confined near the magnetic axis in a region of low magnetic shear, i.e. $(d\ln q/d\ln r) << 1$ for $r \leq \delta_p$. Over this distance, $\hat{\psi} \approx \hat{r}^2$ and the orbit equation can be cast in the compact form,

$$\sigma_\parallel\left(\hat{\lambda} + \hat{r}\cos\vartheta\right)^{1/2} = \hat{r}^2 - \hat{\psi}_\varphi. \tag{1}$$

Non-standard orbits satisfy the inequalities $\hat{\psi}_\varphi \leq 1$, $\hat{\lambda} \leq 1$. We observe that the orbit equation (1) includes the grad-B guiding centre drift, but neglects the magnetic curvature drift, consistently with the non-standard ordering.

The orbit equation (1) is equivalent to the Hamiltonian for guiding centre motion,

$$H(\hat{x}, \hat{y}; \hat{\psi}_\varphi) = (\hat{x}^2 + \hat{y}^2 - \hat{\psi}_\varphi)^2 - \hat{x} = \hat{\lambda}, \tag{2}$$

where the Cartesian coordinates $\hat{x} = \hat{r}\cos\vartheta$, $\hat{y} = \hat{r}\sin\vartheta$ are canonically conjugate variables, with $\hat{x}$ playing the role of the canonical momentum variable and $\hat{\lambda}$ that of the effective energy. The stationary solutions of Hamilton's equations define three curves in the $(\hat{\lambda}, \hat{\psi}_\varphi)$ plane, represented in Fig. 1a: the curve $\hat{\lambda} = \hat{\lambda}_0(\hat{\psi}_\varphi)$, corresponding to the locus of the (stable) co-passing stagnation orbits, where $\sigma_\parallel = +1$; the curve $\hat{\lambda} = \hat{\lambda}_+(\hat{\psi}_\varphi)$, corresponding to (stable) counter-passing stagnation orbits, with $\sigma_\parallel = -1$; the curve $\hat{\lambda} = \hat{\lambda}_-(\hat{\psi}_\varphi)$, corresponding to the locus of the

(unstable) pinch orbits. Along the pinch orbit (Fig. 1b), $v_\parallel$ changes sign, going through zero at the orbit tips, while the pinch point at $\hat{x} = \hat{x}_p$ is an unstable stagnation point. The curves $\hat{\lambda}_\pm$ terminate in a common point, which we refer to as the cusp point, where $\hat{\lambda} = \hat{\psi}_\varphi = 3/4$. The three curves, $\hat{\lambda}_0$ and $\hat{\lambda}_\pm$, subdivide the parameter plane $(\hat{\lambda}, \hat{\psi}_\varphi)$ into three regions. Each point within region I corresponds to two orbits, which are nested into each other; one orbit pertains to each point within region II, while no orbits exist within region III. A more detailed orbit classification on the basis of Eq. (1) can be found in Ref. [6].

All the orbits described by the Hamiltonian (2) are closed in the $(\hat{x}, \hat{y})$ plane. The bounce time, $\tau_b(\hat{\lambda}, \hat{\psi}_\varphi) = \oint d\tau = \oint dx / \dot{x}$, can be evaluated analytically in terms of elliptic integrals. For the pinch orbit, τ_b has a logarithmic singularity (for the special case of the cusp orbit, the inner loop of the pinch orbit degenerates into a point and τ_b diverges algebraically), while τ_b remains finite for the co- and counter-passing stagnation orbits.

If we now consider the collisions of the high energy ions with the thermal plasma, the quantities $\hat{\lambda}$ and $\hat{\psi}_\varphi$ are no longer invariants of the motion. In the high energy limit, i.e. $E > E_{crit} \sim \alpha T_e$ with T_e the electron temperature and $\alpha \sim 10$ a mass-dependent factor, only the collisional drag by the thermal electrons is important. Thus, we are led to consider the simplified Fokker-Planck equation in the drift-kinetic approximation,

$$\partial f / \partial t + \mathbf{v}_{gc} \cdot \nabla f = C(f) + S, \tag{3}$$

where f is the fast ion distribution function, $C(f) = \tau_s^{-1} v^{-2} \partial(v^3 f) / \partial v$ is the collisional drag term, τ_s is the slowing-down time, $\mathbf{v}_{gc}$ is the guiding centre velocity and S is the fast ion source term. Equation (3) assumes the phase-space variables r, ϑ, v and λ. For *MeV* ions and typical parameters of magnetic fusion experiments, the ratio $\delta \equiv \tau_b / \tau_s$ is very small, typically $\delta \sim 10^{-5}$, except in an exponentially thin strip of the $(\hat{\lambda}, \hat{\psi}_\varphi)$ plane around the pinch locus. This suggests the expansion $f = f_0 + (\tau_b / \tau_s) f_1 + \ldots$. To leading order, $\mathbf{v}_{gc} \cdot \nabla f_0 = 0$, thus $f_0 = f_0(v, \lambda, P_\varphi, t)$ can be taken to be a function of the invariants of the collisionless motion. The first order equation reads $\partial f_0 / \partial t + \mathbf{v}_{gc} \cdot \nabla f_1 = C(f_0) + S$. The term involving f_1 is annihilated by bounce averaging. It is convenient to perform first the variable transformation $(r, \vartheta) \rightarrow (P_\varphi, \tau)$, where τ is the time along

the guiding centre orbit. With this transformation, $\mathbf{v}_{gc}\cdot\nabla f \to \partial f/\partial\tau$ and the drag term splits into two parts, $\partial f/\partial \mathrm{v} \to \partial f/\partial \mathrm{v} + [(P_\varphi - Ze\psi/c)/\mathrm{v}]\partial f/\partial P_\varphi$. The last term is usually neglected in the standard orbit approximation. With the further transformation $(\mathrm{v}, P_\varphi) \to (\hat{\lambda}, \hat{\psi}_\varphi)$, the bounce-averaged Fokker-Planck equation takes the form $dF/d\hat{t} = \tau_s \mathrm{v}^3 \langle S \rangle$, where $\hat{t} = t/\tau_s$ (we have assumed for simplicity $\tau_s = \text{const}$), $F = F[\hat{t}, \hat{\psi}_\varphi(\hat{t}), \hat{\lambda}(\hat{t})] \equiv \mathrm{v}^3 f$, and the characteristic equations are

$$\dot{\hat{\psi}}_\varphi = \langle \hat{r}^2 \rangle + \hat{\psi}_\varphi/3, \qquad \dot{\hat{\lambda}} = 2\hat{\lambda}/3, \tag{4}$$

where $\dot{\alpha} \equiv d\alpha/d\hat{t}$ and angle brackets denote bounce averaging, $\langle ... \rangle \equiv \tau_b^{-1} \oint (...) d\tau$. The function $g(\hat{\lambda}, \hat{\psi}_\varphi, \sigma) = \langle \hat{r}^2 \rangle$, which can be expressed in terms of elliptic integrals, is a double-valued function of $(\hat{\lambda}, \hat{\psi}_\varphi)$ within region I of Fig. 1a, hence the need to introduce in this region an index σ which specifies the Riemann sheet: $\sigma = -1$ for the inner orbit and $\sigma = +1$ for the outer orbit. The support for the function $g(\hat{\lambda}, \hat{\psi}_\varphi, -1)$ coincides with region I, which is limited on the left by the curve $\hat{\lambda} = \hat{\lambda}_+$, while the function $g(\hat{\lambda}, \hat{\psi}_\varphi, +1)$ is analytic across this curve. Note that $g(\hat{\lambda}, \hat{\psi}_\varphi, -1) \le g(\hat{\lambda}, \hat{\psi}_\varphi, +1)$. The equality sign applies on the pinch locus, where $g \to \hat{r}_p^2$ reduces to the square of the pinch radius.

Analysis of the characteristic equations (4) reveals the existence of an unstable fixed point at $\hat{\lambda}_f = 0$, $\hat{\psi}_{\varphi f} = -3(16)^{-2/3} \approx -0.47$, which corresponds to a co-passing stagnation orbit located at $\hat{x} = 16^{-1/3}$, $\hat{y} = 0$. The characteristic curves in the $(\hat{\lambda}, \hat{\psi}_\varphi)$ plane can be thought of as originating from this fixed point at $\hat{t} \to -\infty$, as shown in Figs.1c and 1d. Some of these curves intersect the pinch locus. At the intersection point, a branching of the characteristic curves occurs, as represented by the diagram of Fig. 2a. An outer orbit in region I evolves into a pinch orbit. Thereafter, a small perturbation transforms the orbit, either into the adjacent inner orbit in region I, or into the adjacent *trapped* orbit in region II. A third branch, which maps the pinch locus onto itself, is dynamically unstable.

In order to proceed, we must decide which of the two stable branches an orbit will follow. First, we recognise that, while the Hamiltonian (2) describes the guiding centre motion on the fast bounce time scale, where $\hat{\lambda}$ and $\hat{\psi}_\varphi$ can be taken as constant, the characteristic equations (4)

the guiding centre orbit. With this transformation, $\mathbf{v}_{gc}\cdot\nabla f \to \partial f/\partial\tau$ and the drag term splits into two parts, $\partial f/\partial \mathrm{v} \to \partial f/\partial \mathrm{v} + [(P_\varphi - Ze\psi/c)/\mathrm{v}]\partial f/\partial P_\varphi$. The last term is usually neglected in the standard orbit approximation. With the further transformation $(\mathrm{v}, P_\varphi) \to (\hat{\lambda}, \hat{\psi}_\varphi)$, the bounce-averaged Fokker-Planck equation takes the form $dF/d\hat{t} = \tau_s \mathrm{v}^3 \langle S \rangle$, where $\hat{t} = t/\tau_s$ (we have assumed for simplicity $\tau_s = \text{const}$), $F = F[\hat{t}, \hat{\psi}_\varphi(\hat{t}), \hat{\lambda}(\hat{t})] \equiv \mathrm{v}^3 f$, and the characteristic equations are

$$\dot{\hat{\psi}}_\varphi = \langle \hat{r}^2 \rangle + \hat{\psi}_\varphi/3, \qquad \dot{\hat{\lambda}} = 2\hat{\lambda}/3, \tag{4}$$

where $\dot{\alpha} \equiv d\alpha/d\hat{t}$ and angle brackets denote bounce averaging, $\langle ... \rangle \equiv \tau_b^{-1} \oint (...) d\tau$. The function $g(\hat{\lambda}, \hat{\psi}_\varphi, \sigma) = \langle \hat{r}^2 \rangle$, which can be expressed in terms of elliptic integrals, is a double-valued function of $(\hat{\lambda}, \hat{\psi}_\varphi)$ within region I of Fig. 1a, hence the need to introduce in this region an index σ which specifies the Riemann sheet: $\sigma = -1$ for the inner orbit and $\sigma = +1$ for the outer orbit. The support for the function $g(\hat{\lambda}, \hat{\psi}_\varphi, -1)$ coincides with region I, which is limited on the left by the curve $\hat{\lambda} = \hat{\lambda}_+$, while the function $g(\hat{\lambda}, \hat{\psi}_\varphi, +1)$ is analytic across this curve. Note that $g(\hat{\lambda}, \hat{\psi}_\varphi, -1) \le g(\hat{\lambda}, \hat{\psi}_\varphi, +1)$. The equality sign applies on the pinch locus, where $g \to \hat{r}_p^2$ reduces to the square of the pinch radius.

Analysis of the characteristic equations (4) reveals the existence of an unstable fixed point at $\hat{\lambda}_f = 0$, $\hat{\psi}_{\varphi f} = -3(16)^{-2/3} \approx -0.47$, which corresponds to a co-passing stagnation orbit located at $\hat{x} = 16^{-1/3}$, $\hat{y} = 0$. The characteristic curves in the $(\hat{\lambda}, \hat{\psi}_\varphi)$ plane can be thought of as originating from this fixed point at $\hat{t} \to -\infty$, as shown in Figs.1c and 1d. Some of these curves intersect the pinch locus. At the intersection point, a branching of the characteristic curves occurs, as represented by the diagram of Fig. 2a. An outer orbit in region I evolves into a pinch orbit. Thereafter, a small perturbation transforms the orbit, either into the adjacent inner orbit in region I, or into the adjacent *trapped* orbit in region II. A third branch, which maps the pinch locus onto itself, is dynamically unstable.

In order to proceed, we must decide which of the two stable branches an orbit will follow. First, we recognise that, while the Hamiltonian (2) describes the guiding centre motion on the fast bounce time scale, where $\hat{\lambda}$ and $\hat{\psi}_\varphi$ can be taken as constant, the characteristic equations (4)

represent a reduced description for the orbit evolution on the slow (collisional) time scale. Within this description, any information of the quickly varying phases is lost. This description is closed only until the moment of the transition. In order to close the system, it is necessary to introduce integral quantities, the *transition probabilities,* which may depend on $\hat{\lambda}$ and $\hat{\psi}_\varphi$ but not on the orbit phase, and which determine the evolution of the system across the transition region. Let us consider the following argument. The equations of motion are determined by the *time-dependent* Hamiltonian (2), $\hat{\lambda}(\hat{t}) = H[\hat{x}, \hat{y}, \hat{\psi}_\varphi(\hat{t})]$, where $\hat{\psi}_\varphi$ obeys Eqs. (4). With reference to Fig. 1b, we identify the separatrix (the pinch orbit) at a given time, $\hat{t} = \hat{t}_0$, and for given $\hat{\psi}_\varphi(\hat{t}_0)$, $\hat{\lambda} = \hat{\lambda}_-[\hat{\psi}_\varphi(\hat{t}_0)]$, nested into a higher $\hat{\lambda} = \hat{\lambda}_{out}(\hat{t}_0)$ trajectory (an outer orbit). We denote by I_i, $i = A,B,C$, respectively, the areas enclosed by the two lobes of the separatrix and by the strip between the separatrix and the higher $\hat{\lambda}$ trajectory. At a later time, $\hat{t} = \hat{t}_0 + \Delta\hat{t}$, the seperatrix and the new trajectory corresponding to $\hat{\lambda} = \hat{\lambda}_{out}(\hat{t}_0 + \Delta\hat{t})$ will have modified their shapes and so the three areas will have changed (we consider time intervals such that $\hat{\lambda}_{out} > \hat{\lambda}_-$). However, owing to the Liouville theorem, the total area is conserved, $\sum_i I_i = \text{constant}$. The variation of each area within a short period of time is $\Delta I_i = \dot{I}_i(\hat{t}_0)\Delta\hat{t}$. It follows that $\sum_i \dot{I}_i = 0$. Let, for example, I_C decrease, $\dot{I}_C < 0$, so that the phase trajectories leave region C and move into A or B. The probability of transition from C to A or B is determined as the ratio of the measure of all the trajectories moving into A or B to that of all the trajectories leaving C:

$$P_{C\to A} = -\dot{I}_A / \dot{I}_C; \quad P_{C\to B} = -\dot{I}_B / \dot{I}_C. \tag{5}$$

A proof of this, which is referred to as Kruskal's theorem in Ref. [9], can be found, e.g., in Refs. [10-12] . It should be noted that, strictly speaking, the adiabatic approximation breaks down in a very narrow strip around the separatrix. However, it can be shown that this introduces small corrections of order $\delta \ln \delta$ to the transition probabilities in (5).

The computation of $\dot{I}_i$ involves integrals of the type $\oint \hat{y} d\hat{x}$, which can be evaluated analytically, leading to the following expressions for the transition probability functions:

$$P_{C\to A} = \frac{1 - g(\hat{\psi}_\varphi)}{1 + g(\hat{\psi}_\varphi)}; \quad P_{C\to B} = \frac{2g(\hat{\psi}_\varphi)}{1 + g(\hat{\psi}_\varphi)}; \quad g(\hat{\psi}_\varphi) = \frac{2}{\pi}\arcsin\left(\frac{2z_p - z_2 + z_1}{z_2 + z_1}\right), \tag{6}$$

where $z_j = (\hat{\lambda} + \hat{x}_j)^{1/2}$ and x_j , $j = p$, 1, 2 are the roots of $\hat{y}$ (cf. Fig. 1b) Graphs of the transition probabilities along the pinch locus are shown in Fig. 2b. Note that the transition probability to trapped orbits approaches unity near the cusp orbit at $\hat{\psi}_\varphi = 3/4$. Transitions to the inner orbit become increasingly more likely at larger values of $\hat{\psi}_\varphi$, i.e. grows in the standard orbit limit.

Let us now illustrate the effects of slowing down and branching by studying the injection of a mono-energetic neutral beam. We assume co-injection at a constant angle, $\alpha_{inj} = 56^0$ ($\cos\alpha_{inj} = v_\perp / v$) and ionisation in a narrow layer on the low field side of the midplane ($\vartheta = 0$). The source is taken to be Gaussian, $S \sim \delta(\vartheta)\exp\left\{-\left[(\hat{r} - \hat{r}_{inj})/\Delta\hat{r}\right]^2\right\}\delta(v - v_0)$, with parameters $\hat{r}_{inj} = 1.4$, $\Delta\hat{r} = 0.2$..

The flux surface averaged density profile of injected ions is given by $n(r,t) = (m^2 r R_0)^{-1}\int f(E,\mu,P_\varphi,t)(d\tau/dr)dEd\mu dP_\varphi$, where $d\tau$ is the bounce time differential. The time evolution of $n(r,t)$ for the considered source is shown in Fig. 3a., Note the build up in time of the density near the magnetic axis. In Fig. 3b, the characteristic followed by orbits born at $\hat{r} = \hat{r}_{inj}$ is shown. For this characteristic, the probability of transition to trapped orbits is about 27%. Figures 3c and 3d portray examples of ion orbits at various times along this characteristic. It can be seen that immediately after branching, the inner counter-passing orbit, as well as the inner leg of the trapped orbit, are located on the high field side. When ions on inner orbits slow down, they drift inward, encircle the magnetic axis and eventually become standard passing ions. Likewise, the inner leg of the trapped ion orbit intersects the magnetic axis during slowing down. These two effects combine to produce the observed build up of the average fast ion density in the centre. A reduction of the average $\langle r^2 \rangle$ during slowing down does not apply only to special orbits on branching characteristics, but more in general to all those orbits, co- and counter-passing as well as trapped orbits, which remain within the non-standard region $r \le \delta_p(E)$, for a long enough time as they slow down in energy. Such are, for instance, all the orbits born with values of $\hat{\psi}_\varphi$ and $\hat{\lambda}$ in the vicinity of the fixed point of Fig. 1c. The relevant time can be taken to be the time to slow down from the initial energy, $E_0 = \mathcal{O}(1MeV)$, to the energy, E_{crit}, at which pitch angle scattering by background ions becomes important. Then, for typical values of Tokamak experiments, the characteristic distance from the magnetic axis within which non-standard fast ion

orbits remain confined shrinks by a factor $\delta_p(E_{crit})/\delta_p(E_0) = (E_{crit}/E_0)^{1/3} \sim 0.5$ before thermalization.

The authors would like to thank H.L.Berk, S.Bulanov and M.Ottaviani for useful discussions.

References

[1] B.B.Kadomtsev and O.P.Pogutse, *Zh.Eksp.Teor.Fiz.* **51**, 1734 (1966) [Soviet Phys. JETP **24**, 1172 (1967)].

[2] L.M.Hively, G.H.Miley and J.A.Rome, *Nuclear Fusion* **21**, 1431 (1981).

[3] V.Ya Goloborod'ko, Ya.I.Kolesnichenko and V.O.Yavorskij, *Nuclear Fusion* **23**, 399 (1983).

[4] F.S.Zaitsev, M.R.O'Brien and M.Cox, *Phys. Fluids B* **5**, 509 (1993).

[5] Ya.I.Kolesnichenko et al, Chalmers Univ. of Technology Report: CTH-IEFT//PP-1994-12, also submitted to *Plasma Physics and Controlled Fusion.*

[6] F.Porcelli, L.-G.Eriksson and H.L.Berk, in *Proc. 21st EPS Conference on Contr. Fusion and Plasma Physics* (Montpellier, 1994), Vol. II, p. 648.

[7] T.E.Stringer, *Plasma Physics* **16**, 651 (1974).

[8] J.A.Rome and Y.-K.M.Peng, *Nuclear Fusion* **19**, 1193 (1979).

[9] D.Dobrott and J.M.Greene, *Phys. Fluids* **14**, 1525 (1971).

[10] A.S.Bakaj, in *Asymptotic Analysis II,* Vol 985 of *Lecture Notes in Mathematics,* Ed. F. Verhulst (Springer, New York, 1983), p 96.

[11] J.R.Cary, D.F.Escande and J.L.Tennyson, *Physical Review A* **34**, 4256 (1986).

[12] A.V.Timofeev, *Zh. Eksp. Teor. Fiz.* **75**, 1303 (1978) [*Sov. Phys. JETP* **48**, 656 (1978)].

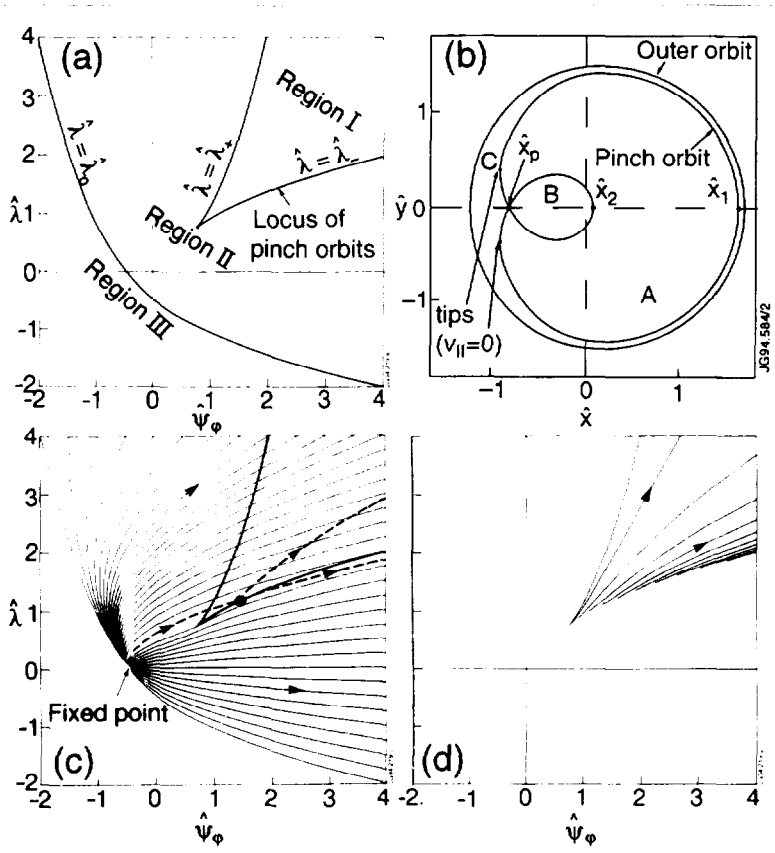

Fig. 1. (a) Parameter plane $(\hat{\lambda}, \hat{\psi}_\varphi)$, subdivided into three regions by the curves $\hat{\lambda} = \hat{\lambda}_0$, and $\hat{\lambda} = \hat{\lambda}_\pm$, corresponding to the stationary curves of the Hamiltonian (2); (b) Pinch orbit for $\hat{\psi}_\varphi = 1$, $\hat{\lambda} = 0.927$, nested into an outer orbit with $\hat{\psi}_\varphi = 1$, $\hat{\lambda} = 1.5$. $\hat{x}_2$, $\hat{x}_1$, and $\hat{x}_p$ are the coordinates of the intersections of the pinch orbit with the poloidal midplane ($\hat{x}_p$ is the pinch point); (c) Characteristic curves in the $(\hat{\lambda}, \hat{\psi}_\varphi)$ plane. The arrows indicate the direction of time. A branching characteristic is exemplified by the dashed curve; (d) Characteristic curves for the inner orbits within region I.

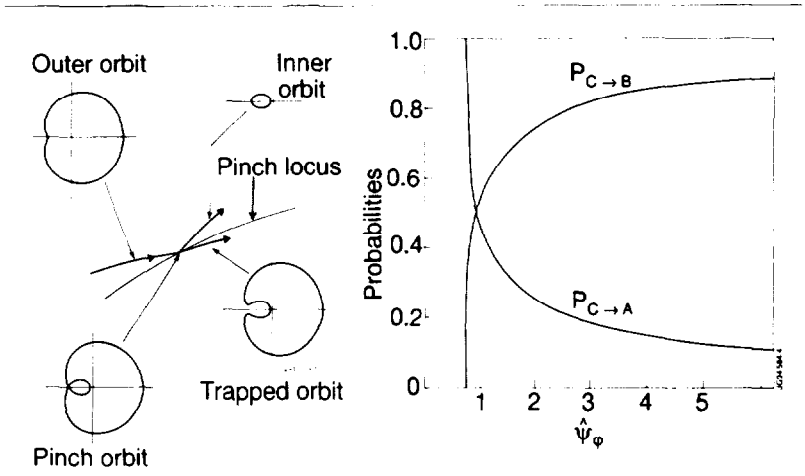

Fig. 2 (a) Branching diagram; (b) Transition probabilities as functions of $\hat{\psi}_\varphi$ along the pinch locus.

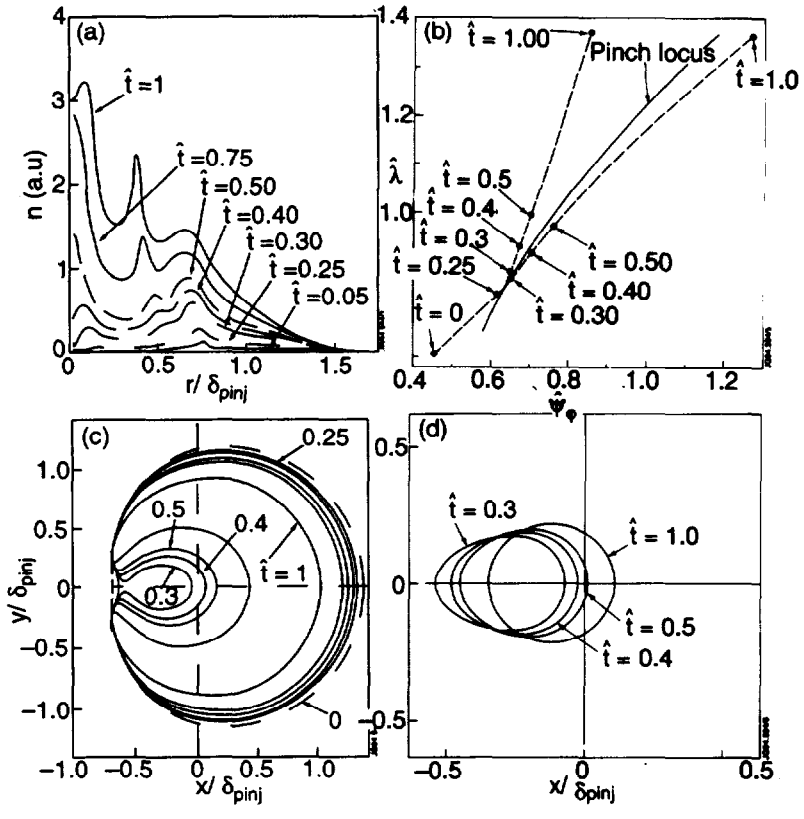

Fig. 3. (a) Density profile at various normalised times $\hat{t} = t/t_s$; (b) Branching characteristic for injected ions with $\hat{r} = \hat{r}_{inj}$; (c) Orbit evolution following the trapped branch. The initial orbit (dashed line) and the orbit at $\hat{t}$ = 0.25 are before branching; (d) Orbit evolution following the inner orbit.